**Mechanics of Dynamic Debonding**

W. Yang, Z. Suo, C. F. Shih

*Proceedings: Mathematical and Physical Sciences*, Volume 433, Issue 1889 (Jun. 8, 1991), 679-697.

Your use of the JSTOR database indicates your acceptance of JSTOR's Terms and Conditions of Use. A copy of JSTOR's Terms and Conditions of Use is available at http://www.jstor.org/about/terms.html, by contacting JSTOR at jstor-info@umich.edu, or by calling JSTOR at (888)388-3574, (734)998-9101 or (FAX) (734)998-9113. No part of a JSTOR transmission may be copied, downloaded, stored, further transmitted, transferred, distributed, altered, or otherwise used, in any form or by any means, except: (1) one stored electronic and one paper copy of any article solely for your personal, non-commercial use, or (2) with prior written permission of JSTOR and the publisher of the article or other text.

Each copy of any part of a JSTOR transmission must contain the same copyright notice that appears on the screen or printed page of such transmission.

*Proceedings: Mathematical and Physical Sciences* is published by The Royal Society. Please contact the publisher for further permissions regarding the use of this work. Publisher contact information may be obtained at http://www.jstor.org.

*Proceedings: Mathematical and Physical Sciences*
©1991 The Royal Society

JSTOR and the JSTOR logo are trademarks of JSTOR, and are Registered in the U.S. Patent and Trademark Office. For more information on JSTOR contact jstor-info@umich.edu.

©2001 JSTOR

http://www.jstor.org/
Mon Jan 22 22:46:04 2001

# Mechanics of dynamic debonding

By W. Yang[1], Z. Suo[2] and C. F. Shih[3]

[1] *Department of Engineering Mechanics, Tsinghua University, Beijing 100084, People's Republic of China*

[2] *Department of Mechanical Engineering, University of California, Santa Barbara, California 93106, U.S.A.*

[3] *Division of Engineering, Brown University, Providence, Rhode Island 02912, U.S.A.*

Singular fields around a crack running dynamically along the interface between two anisotropic substrates are examined. Emphasis is placed on extending an established framework for interface fracture mechanics to include rapidly applied loads, fast crack propagation and strain rate dependent material response. For a crack running at non-uniform speed, the crack tip behaviour is governed by an instantaneous steady-state, two-dimensional singularity. This simplifies the problem, rendering the Stroh techniques applicable. In general, the singularity oscillates, similar to quasi-static cracks. The oscillation index is infinite when the crack runs at the Rayleigh wave speed of the more compliant material, suggesting a large contact zone may exist behind the crack tip at high speeds. In contrast to a crack in homogeneous materials, an interface crack has a finite energy factor at the lower Rayleigh wave speed. Singular fields are presented for isotropic bimaterials, so are the key quantities for orthotropic bimaterials. Implications on crack branching and substrate cracking are discussed. Dynamic stress intensity factors for anisotropic bimaterials are solved for several basic steady state configurations, including the Yoffe, Gol'dshtein and Dugdale problems. Under time-independent loading, the dynamic stress intensity factor can be factorized into its equilibrium counterpart and the universal functions of crack speed.

## 1. Introduction

It is well known that the mechanical behaviour and the overall performance of many newly developed multiphase materials are largely controlled by the response of the interfaces. For this reason, an interface fracture mechanics approach for treating debonding is crucial to the emerging technology of designing and manufacturing multiphase materials. The methodology can be used to guide material selection and assess the effects of processing on debonding toughness.

The body of recently obtained theoretical and experimental results that is the basis of an interface fracture mechanics methodology is reviewed by Ruhle *et al.* (1990). The field has been driven largely by pressing engineering problems such as thin film adhesion and brittle composite toughening. In many of these material systems the low ductility or brittleness is caused by fracture that invariably begin at the interfaces under mixed mode conditions. The confrontation with this reality motivates a pragmatic approach, which views the debonding resistance as a function of the mode mixity. The approach has been rationalized by Rice (1988) on the basis of small-scale-contact and $K$-annulus, and by Evans *et al.* (1990) with many

*Proc. R. Soc. Lond.* A (1991), **433**, 679–697
*Printed in Great Britain*

technically representative systems tested. The approach has been further advanced by Hutchinson & Suo (1991) with analysis carried out for layered materials of many varieties. Suo (1990) and Wang *et al.* (1991) have extended the approach to include anisotropy typical of composite laminates.

Despite its obvious importance, we have little understanding of the dynamic aspects of debonding: material inertia, strain rate sensitivity, and debonding speed. When a polymer composite laminate experiences an impact, the matrix splits and delamination follows. The pattern and the extent of debonding, and therefore the impact damage tolerance, are strongly affected by the rate of loading, the mode mixity and the strain rate sensitivity of the material. These observations notwithstanding, the response of the layered materials is often evaluated on the basis of static fracture mechanics. It is not surprising that a coherent account of dynamic effects has yet to emerge.

Inertial effects can arise from rapidly applied loading or from fast crack propagation and plays an important role in affecting the load transfer characteristics in the structure and the mode mixity. Indeed loading rate and mode mixity strongly affects the fracture process in rate sensitive materials. In a PMMA-aluminium debonding test, Tippur & Rosakis (1990) observed the debonding crack runs at 80% of the Rayleigh wave speed of PMMA, a speed hardly achievable should the crack run in a homogeneous PMMA. The attempt to explain this, and to understand the damage in composites caused by impact loading instigated our interest in this area.

The mathematical analysis to be presented builds on earlier works on the subject, particularly by Gol'dshtein (1966), Willis (1971) and Atkinson (1977). The complex-variable representation of Stroh (1962) and several ideas of Suo (1990) are integrated to capture the singularity structure. Solutions are reinterpreted in the light of the pragmatic approach for interface debond emerged in recent years. Effort is made to unify various entities of elastic fracture: statics, dynamics, heterogeneity, and anisotropy.

The plan of the paper is as follows. In §2, we argue that for cracks running at nonuniform speed, the near tip singularity is two dimensional, and instantaneously in a steady state. Stroh formulation is therefore suitable to solve for the crack tip field. In fact most results are obtained, by analogy, from the static ones in Suo (1990). Explicit results are presented for isotropic and orthotropic bimaterials. A compliance-like matrix, $\boldsymbol{H}$, depending on crack speed and elastic constants, unifies concepts in interface fracture. The singularity structure for both real and complex $\boldsymbol{H}$ are discussed in §3. Angular functions for isotropic bimaterials are extracted. Features unique to dynamic interface cracks are noted. These features may lead to events different from either low speed debonding, or high speed crack propagation in homogeneous materials. In §4, we show that the oscillation index becomes infinite when crack approaches the Rayleigh wave speed of the more compliant material. Consequently, the concept of small scale contact is invalid at high speeds. The energy factor for bimaterials is finite at the lower Rayleigh wave speed. The velocity dependence of these parameters are plotted for isotropic bimaterials. Section 5 catalogues the dynamic stress intensity factors. Solutions for general anisotropic bimaterials are obtained. A factorization is constructed for the dynamic interface stress intensity factor for uniform crack motion under time-independent loading.

## 2. Local steady state and Stroh formulation

### 2.1. *Steady-state two-dimensional singularity*

Figure 1 shows a planar interface crack. Materials 1 and 2 occupy the two halfspaces. The Navier equations governing the displacements $u_1, u_2, u_3$ are

$$C_{ijkl}\,\partial^2 u_k/\partial x_l\,\partial x_i = \rho\ddot{u}_j. \tag{2.1}$$

The stiffness tensor $C_{ijkl}$ and material density $\rho$ take on different values for the two substrates. Superscripts $(\,)^{(1)}$ are $(\,)^{(2)}$ will be attached when distinction is necessary. The tensor $C_{ijkl}$ is positive definite and possesses the Voigt symmetry. Material 1 is assumed to have a lower Rayleigh wave speed, designated as $c_{\mathrm{R}}$. Suppose the crack runs at speed $v = \dot{l}(t)$ smaller than $c_{\mathrm{R}}$.

The coordinates $\hat{x}_i$ translating with the crack tip are

$$\hat{x}_1 = x_1 - l(t), \quad \hat{x}_2 = x_2, \quad \hat{x}_3 = x_3. \tag{2.2}$$

For the singular field near the crack tip, among the four partial derivatives in the new coordinates, $\partial u_k/\partial\hat{x}_3$ and $\partial u_k/\partial t$ are less singular than $\partial u_k/\partial\hat{x}_1$ and $\partial u_k/\partial\hat{x}_2$. Consequently, the leading term of the acceleration is

$$\ddot{u}_j = v^2 u_{j,11}. \tag{2.3}$$

The Navier equation (2.1), for the leading singularity, reduces to

$$\hat{C}_{\alpha jk\beta}\,u_{k,\alpha\beta} = 0, \quad \alpha,\beta = 1,2, \tag{2.4}$$

where $(\,)_{,\alpha} = \partial(\,)/\partial\hat{x}_\alpha$. The effective elastic constants depend on crack speed

$$\hat{C}_{\alpha jk\beta} = C_{\alpha jk\beta} - \rho v^2 \delta_{jk}\,\delta_{1\alpha}\,\delta_{1\beta}, \tag{2.5}$$

where $\delta_{ij}$ is the Kronecker delta. Note $\hat{C}_{\alpha jk\beta}$ does not possess the Voigt symmetry, but is invariant for a complete reverse of the indices, i.e.

$$\hat{C}_{\beta kj\alpha} = \hat{C}_{\alpha jk\beta}. \tag{2.6}$$

Equation (2.4) describes a two-dimensional field on the $(\hat{x}_1, \hat{x}_2)$-plane, with no explicit dependence on time $t$. Accordingly, the crack tip at each instance experiences a steady-state two-dimensional singularity. The above argument is the same as that used by Rice (1968) for cracks in homogeneous materials.

### 2.2. *Stroh formulation*

The planar partial differential equations (2.4) can be solved by a complex-variable representation due to Stroh (1962). Stress functions, $\Phi_i$, are defined such that

$$\sigma_{1i} = -\Phi_{i,2} + \rho v^2 u_{i,1}, \quad \sigma_{2i} = \Phi_{i,1}. \tag{2.7}$$

The displacements and stress functions, $u_i$ and $\Phi_i$, are linear in three analytic functions $f_q$

$$u_i = 2\,\mathrm{Re}\left\{\sum_{q=1}^{3} A_{iq} f_q(z_q)\right\}, \quad \Phi_i = 2\,\mathrm{Re}\left\{\sum_{q=1}^{3} L_{iq} f_q(z_q)\right\}. \tag{2.8}$$

The complex arguments take the form

$$z_q = \hat{x}_1 + p_q \hat{x}_2. \tag{2.9}$$

Substituting (2.8$a$) into (2.4) yields an eigenvalue problem,

$$\sum_{q=1}^{3} \{\hat{C}_{1ik1} + p_q(\hat{C}_{1ik2} + \hat{C}_{2ik1}) + p_q^2 \hat{C}_{2ik2}\} A_{kq} = 0. \tag{2.10}$$

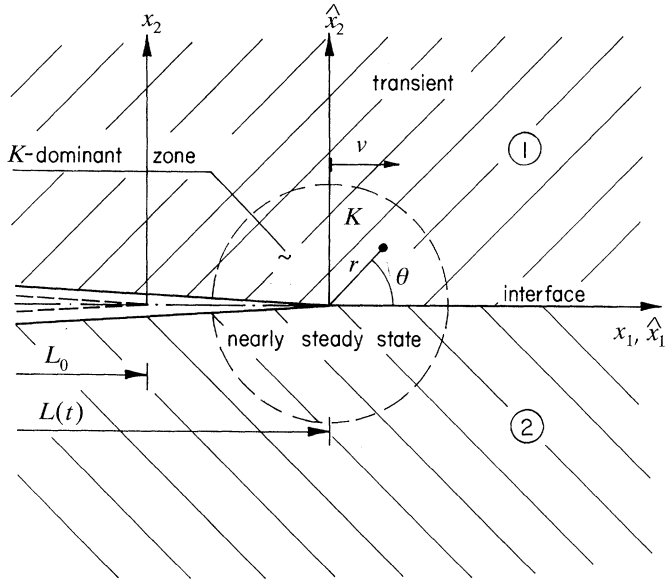


Figure 1. A bimaterial interface crack advancing dynamically under mixed mode loading. The fixed coordinates and the translating coordinates are indicated in the figure.

The eigenvalues $p_q$ are roots of the sixth-order polynomial

$$\det\{\hat{C}_{1ij1}+p_q(\hat{C}_{1ij2}+\hat{C}_{2ij1})+p_q^2\hat{C}_{2ij2}\}=0, \tag{2.11}$$

where $\det\{\}$ denotes the determinant. When $v < c_R$, all eigenvalues are complex and form three conjugate pairs. The three roots with positive imaginary parts are chosen, designated as $p_1$, $p_2$ and $p_3$. The normalization of each column of matrix $\boldsymbol{A}$ is arbitrary. Combining (2.7) and (2.8) gives

$$L_{iq}=\sum_{j=1}^{3}\{\hat{C}_{2ij1}+p_q\hat{C}_{2ij2}\}A_{jq}=-\sum_{j=1}^{3}\{p_q^{-1}\hat{C}_{1ij1}+\hat{C}_{1ij2}\}A_{jq}. \tag{2.12}$$

The traction vector on planes parallel to the interface is

$$\sigma_{2i}=2\,\mathrm{Re}\sum_{q=1}^{3}L_{iq}f_q'(z_q). \tag{2.13}$$

The basic equations for the steady-state fields, (2.8)–(2.13), are identical to those for the static problem when $\hat{x}_i$ and $\hat{C}_{ijkl}$ are identified with $x_i$ and $C_{ijkl}$. Accordingly, static results carry over to the dynamic analysis. The strategy has been adopted by Willis (1971). Most results presented in subsequent sections are obtained, by analogy, from the static solutions in Suo (1990). (After the completion of this work, we found Wu (1990) addressed several issues in §§2 and 3 of this manuscript. Results contained in our sections are relatively complete and explicit.)

Two compliance-like hermitian matrices central to the analysis, $\boldsymbol{B}$ and $\boldsymbol{H}$, are defined by

$$\boldsymbol{B}=\mathrm{i}\boldsymbol{A}\boldsymbol{L}^{-1},\quad \boldsymbol{H}=\boldsymbol{B}^{(1)}+\bar{\boldsymbol{B}}^{(2)}, \tag{2.14}$$

where $\mathrm{i}=\sqrt{-1}$, a superposed bar denotes complex conjugate, and standard matrix operations are implied. Note matrix $\boldsymbol{B}$, and consequently $\boldsymbol{H}$, are unaffected by the normalization of $\boldsymbol{A}$ in the eigenvalue problem (2.10). The matrix $\boldsymbol{H}$, having the dimension of compliance, characterizes the interface behaviour.

Observe that $\boldsymbol{B} = \boldsymbol{Z}^{-1}$, where $\boldsymbol{Z}$ is the *surface impedance matrix* (Ingebrigtsen & Tonning, 1969). The *Stoneley wave* speed is determined by (Barnett *et al.* 1985)

$$\det\{\boldsymbol{Z}^{(1)} + \bar{\boldsymbol{Z}}^{(2)}\} = 0, \tag{2.15}$$

and the Rayleigh wave speed in medium 1 is determined from (Lothe & Barnett 1976)

$$\det\{\boldsymbol{Z}^{(1)}\} = 0. \tag{2.16}$$

The Stoneley wave speed is always larger than the Rayleigh wave speed of either substrate (Barnett *et al.* 1985), roughly reflecting the fact that the presence of an adjoining half-space increases stiffness (relative to that of a vacuum) and consequently raises the interfacial wave speed.

### 2.3. *Important cases*

Explicit results for materials with practical significance are gathered here. The conventional 6 by 6 stiffness matrix is used. When $(x_1, x_2)$ is a mirror plane of the material, the governing equation (2.4) decouples into antiplane shear and the plane strain problems. They are treated separately as follows.

#### 2.3.1. *Antiplane shear*

The problem is governed by a single equation for $u_3$. The characteristic number is

$$p_3 = -C_{45}/C_{44} + \mathrm{i}[(C_{55} - \rho v^2)/C_{44} - (C_{45}/C_{44})^2]^{\frac{1}{2}}. \tag{2.17}$$

Only the '33' components of the matrices are non-trivial:

$$A_{33} = 1, \quad B_{33} = \mathrm{i}/L_{33} = \{C_{44}(C_{55} - \rho v^2) - C_{45}^2\}^{-\frac{1}{2}}. \tag{2.18}$$

The Rayleigh wave speed is

$$c_{\mathrm{R}} = [(C_{44}C_{55} - C_{45}^2)/(\rho C_{44})]^{\frac{1}{2}}. \tag{2.19}$$

#### 2.3.2. *Orthotropic materials*

We direct attention to in-plane deformation. The relevant elastic constants are

$$\begin{pmatrix} C_{11} & C_{12} & 0 \\ C_{12} & C_{22} & 0 \\ 0 & 0 & C_{66} \end{pmatrix}. \tag{2.20}$$

Introduce $$\lambda_\gamma = (\rho_{11}\alpha_1^2 + p_\gamma^2)/(\rho_{12} + 1)\, p_\gamma, \quad \gamma = 1, 2. \tag{2.21}$$

Here the stiffness ratios and the wave reduction factors are

$$\rho_{\gamma\beta} = \frac{C_{\gamma\beta}}{C_{66}}, \quad \alpha_1 = \sqrt{\left(1 - \frac{\rho v^2}{C_{11}}\right)}, \quad \alpha_2 = \sqrt{\left(1 - \frac{\rho v^2}{C_{66}}\right)}. \tag{2.22}$$

The eigenvalues $p_1$ and $p_2$, with positive imaginary parts, are the roots of the fourth-order polynomial

$$p^4 + 2s\xi p^2 + \xi^2 = 0 \tag{2.23a}$$

where $$\xi = \alpha_1\alpha_2\sqrt{(\rho_{11}/\rho_{22})}, \quad s = \frac{\alpha_2^2 + \rho_{11}\rho_{22}\alpha_1^2 - (1+\rho_{12})^2}{2\sqrt{(\rho_{11}\rho_{22})}\,\alpha_1\alpha_2}. \tag{2.23b}$$

It can be shown that $\xi > 0$ and $s > -1$ for thermodynamically admissible elastic constants. The roots are

$$p_1, p_2 = \begin{cases} \mathrm{i}\sqrt{\xi}([\tfrac{1}{2}(s+1)]^{\frac{1}{2}} \pm [\tfrac{1}{2}(s-1)]^{\frac{1}{2}}), & \text{if} \quad s \geqslant 1, \\ \sqrt{\xi}(\pm[\tfrac{1}{2}(1-s)]^{\frac{1}{2}} + \mathrm{i}[\tfrac{1}{2}(1+s)]^{\frac{1}{2}}), & \text{if} \quad -1 < s < 1. \end{cases} \tag{2.24}$$

The matrices are

$$\boldsymbol{A} = \begin{pmatrix} 1 & -\lambda_2^{-1} \\ -\lambda_1 & 1 \end{pmatrix}, \quad \boldsymbol{L} = C_{66} \begin{pmatrix} p_1 - \lambda_1 & 1 - p_2/\lambda_2 \\ \rho_{12} - \rho_{22} p_1 \lambda_1 & -\rho_{12}/\lambda_2 + \rho_{22} p_2 \end{pmatrix} \tag{2.25}$$

and

$$\boldsymbol{B} = \frac{1}{C_{66} R} \begin{pmatrix} \rho_{22} \alpha_2^2 [2(1+s)/\xi]^{\frac{1}{2}} & \mathrm{i}(\rho_{22} - \rho_{12} \alpha_2^2/\xi) \\ -\mathrm{i}(\rho_{22} - \rho_{12} \alpha_2^2/\xi) & \rho_{22} [2\xi(1+s)]^{\frac{1}{2}} \end{pmatrix}. \tag{2.26}$$

The generalized Rayleigh wave function $R$ is given by

$$R = \rho_{22}(\rho_{22} \xi - 1 + \alpha_2^2) - \rho_{12}^2 \alpha_2^2/\xi. \tag{2.27}$$

The Rayleigh wave speed $c_{\mathrm{R}}$ is solved from $R = 0$. Observe the matrix $\boldsymbol{H}$ consists of three independent real coefficients $H_{\alpha\beta}$:

$$\boldsymbol{H} = \begin{pmatrix} H_{11} & \mathrm{i}H_{12} \\ -\mathrm{i}H_{12} & H_{22} \end{pmatrix}. \tag{2.28}$$

2.3.3. *Isotropic materials*

For completeness, we list the classical results for isotropic materials. Elastic constants are now related by

$$C_{11} = C_{22}, \quad C_{12} = C_{11} - 2C_{66}. \tag{2.29}$$

The Stroh's eigenvalues and matrices reduce to

$$\left.\begin{aligned} p_1 &= \mathrm{i}\alpha_1, \quad p_2 = \mathrm{i}\alpha_2 \\ \boldsymbol{A} &= \begin{pmatrix} 1 & -\mathrm{i}\alpha_2 \\ \mathrm{i}\alpha_1 & 1 \end{pmatrix}, \quad \boldsymbol{L} = \mu \begin{pmatrix} 2\mathrm{i}\alpha_1 & 1 + \alpha_2^2 \\ -(1+\alpha_2^2) & 2\mathrm{i}\alpha_2 \end{pmatrix}, \\ \boldsymbol{B} &= \frac{1}{\mu D} \begin{pmatrix} \alpha_2(1-\alpha_2^2) & \mathrm{i}(1+\alpha_2^2 - 2\alpha_1\alpha_2) \\ -\mathrm{i}(1+\alpha_2^2 - 2\alpha_1\alpha_2) & \alpha_1(1-\alpha_2^2) \end{pmatrix}. \end{aligned}\right\} \tag{2.30}$$

The Rayleigh wave function $D$ is

$$D = 4\alpha_1\alpha_2 - (1+\alpha_2^2)^2. \tag{2.31}$$

## 3. Crack tip fields

### 3.1. *Real* $\boldsymbol{H}$

For cracks in homogeneous materials and some special bimaterials, $\boldsymbol{H}$ is real, or,

$$\boldsymbol{H} = \bar{\boldsymbol{H}}. \tag{3.1}$$

The singularity assumes a simple structure for this case. The stresses are square root singular, and linear in the three stress intensity factors $K_{\mathrm{I}}$, $K_{\mathrm{II}}$ and $K_{\mathrm{III}}$

$$\sigma_{ij} = (2\pi r)^{-\frac{1}{2}} [K_{\mathrm{I}} \tilde{\sigma}_{ij}^{\mathrm{I}}(\theta) + K_{\mathrm{II}} \tilde{\sigma}_{ij}^{\mathrm{II}}(\theta) + K_{\mathrm{III}} \tilde{\sigma}_{ij}^{\mathrm{III}}(\theta)]. \tag{3.2}$$

The angular functions depend on crack speed and elastic constants of material 1 for a point above the interface, and material 2 below.

With the interface traction vector, $\boldsymbol{t} = \{\sigma_{21}, \sigma_{22}, \sigma_{23}\}$, the three stress intensity factors should be grouped as $\boldsymbol{k} = \{K_{\mathrm{II}}, K_{\mathrm{I}}, K_{\mathrm{III}}\}$. The near-tip traction vector can be rewritten as

$$\boldsymbol{t}(r) = \boldsymbol{k}/\sqrt{(2\pi r)}. \tag{3.3}$$

The mode mixity is fully specified by two solid angles, $\psi$ and $\phi$, in the space of the traction vector,

$$\tan\psi \equiv \lim_{r\to 0}\frac{\sigma_{12}}{\sigma_{22}} = \frac{K_{\mathrm{II}}}{K_{\mathrm{I}}}, \quad \cos\phi \equiv \lim_{r\to 0}\frac{\sigma_{23}}{|t|} = \frac{K_{\mathrm{III}}}{\sqrt{(K_{\mathrm{I}}^2+K_{\mathrm{II}}^2+K_{\mathrm{III}}^2)}}. \tag{3.4}$$

The displacement jump a distance $r$ behind the crack tip, $\boldsymbol{\delta} = \{\delta_1, \delta_2, \delta_3\}$, is linear in $\boldsymbol{k}$

$$\boldsymbol{\delta}(r) = \sqrt{(2r/\pi)}\,\boldsymbol{H}\boldsymbol{k}, \tag{3.5}$$

while the energy release rate $\mathcal{G}$ is quadratic in $\boldsymbol{k}$

$$\mathcal{G} = \tfrac{1}{4}\boldsymbol{k}^{\mathrm{T}}\boldsymbol{H}\boldsymbol{k}. \tag{3.6}$$

The above is derived using Irwin's closure integral (Irwin 1960). As an example, the hermitian matrix $\boldsymbol{H}$ is diagonal for aligned orthotropic materials so that the energy release rate is given by

$$\mathcal{G} = \tfrac{1}{4}(H_{22}K_{\mathrm{I}}^2 + H_{11}K_{\mathrm{II}}^2 + H_{33}K_{\mathrm{III}}^2). \tag{3.7}$$

## 3.2. *Complex* $\boldsymbol{H}$

### 3.2.1. *General solution*

The structure of the crack tip field for complex $\boldsymbol{H}$ is governed by an algebraic eigenvalue problem

$$\bar{\boldsymbol{H}}\boldsymbol{w} = \mathrm{e}^{2\pi\epsilon}\boldsymbol{H}\boldsymbol{w}. \tag{3.8}$$

The three eigenpairs have the form $(\epsilon, \boldsymbol{w})$, $(-\epsilon, \bar{\boldsymbol{w}})$, $(0, \boldsymbol{w}_3)$. The *oscillation index* $\epsilon$ is given by (Ting 1986)

$$\epsilon = (2\pi)^{-1}\ln[(1-\beta)/(1+\beta)], \quad \beta = -\sqrt{(-\tfrac{1}{2}\mathrm{tr}\{[\mathrm{Im}\boldsymbol{H}(\mathrm{Re}\boldsymbol{H})^{-1}]^2\})}, \tag{3.9}$$

where $\mathrm{tr}\{\cdot\}$ denotes matrix trace, and $\beta$ is a generalized Dundurs's parameter. Eigenvectors $\boldsymbol{w}$ and $\boldsymbol{w}_3$ are complex and real respectively, and taken to be dimensionless.

The crack-tip field is a linear combination of two types of singularities: a coupled oscillatory field scaled by a complex $K$, and a non-oscillatory field scaled by a real $K_3$,

$$\sigma_{ij} = \frac{\mathrm{Re}\{Kr^{\mathrm{i}\epsilon}\}}{\sqrt{(2\pi r)}}\tilde{\sigma}_{ij}^1(\theta) + \frac{\mathrm{Im}\{Kr^{\mathrm{i}\epsilon}\}}{\sqrt{(2\pi r)}}\tilde{\sigma}_{ij}^2(\theta) + \frac{K_3}{\sqrt{(2\pi r)}}\tilde{\sigma}_{ij}^3(\theta). \tag{3.10}$$

Here the real and dimensionless angular functions depend on the elastic constants and crack speed. Explicit results will be provided later for isotropic bimaterials.

Projecting the actual interfacial traction $\boldsymbol{t} = \{\sigma_{2i}\}$ onto the eigenvectors as

$$\boldsymbol{t} = t\boldsymbol{w} + \bar{t}\bar{\boldsymbol{w}} + t_3\boldsymbol{w}_3 \tag{3.11}$$

leads to the generalized components of the traction vector $t$, $\bar{t}$ and $t_3$, where $t = t_2 + \mathrm{i}t_1$ is complex and $t_3$ is real. As $r\to 0$, the two components asymptote to

$$t(r) = Kr^{\mathrm{i}\epsilon}/\sqrt{(2\pi r)}, \quad t_3(r) = K_3/\sqrt{(2\pi r)}. \tag{3.12}$$

Mode mixity can be defined using these components, and an example will be given in the next subsection.

The crack face displacement jump is

$$\boldsymbol{\delta}(r) = (\boldsymbol{H}+\bar{\boldsymbol{H}})\sqrt{\left(\frac{r}{2\pi}\right)}\left[\frac{Kr^{\mathrm{i}\epsilon}\boldsymbol{w}}{(1+2\mathrm{i}\epsilon)\cosh\pi\epsilon} + \frac{\bar{K}r^{-\mathrm{i}\epsilon}\bar{\boldsymbol{w}}}{(1-2\mathrm{i}\epsilon)\cosh\pi\epsilon} + K_3\boldsymbol{w}_3\right]. \tag{3.13}$$

The energy release rate is related to $K$ and $K_3$,

$$\mathscr{G} = \frac{\bar{\boldsymbol{w}}^{\mathrm{T}}(\boldsymbol{H}+\bar{\boldsymbol{H}})\,\boldsymbol{w}}{4\cosh^2 \pi\epsilon}|K|^2 + \tfrac{1}{8}\boldsymbol{w}_3^{\mathrm{T}}(\boldsymbol{H}+\bar{\boldsymbol{H}})\,\boldsymbol{w}_3 K_3^2. \tag{3.14}$$

Note the contributions from the two singularities are additive.

3.2.2. *Aligned orthotropic bimaterials*

The in-plane components of $\boldsymbol{H}$ assume the simple form in (2.28). The out-of-plane deformation is uncoupled from the in-plane mode. Using (3.9), we can write the generalized Dundurs's parameter $\beta$ more explicitly as

$$\beta = -H_{12}(H_{11}H_{22})^{-\frac{1}{2}}. \tag{3.15}$$

A close form relationship between $\epsilon$ and the crack speed $v$ can thus be obtained.

The eigenvectors $\boldsymbol{w}$ and $\boldsymbol{w}_3$ have the form

$$\boldsymbol{w} = \tfrac{1}{2}\{-\mathrm{i}\eta, 1, 0\}, \quad \boldsymbol{w}_3 = \{0, 0, 1\}, \quad \eta = (H_{22}/H_{11})^{\frac{1}{2}}, \tag{3.16}$$

where $\eta$ is the *traction resolution factor*. Using (3.16) in (3.11), gives the generalized traction

$$t = \sigma_{22} + \mathrm{i}\sigma_{21}/\eta, \quad t_3 = \sigma_{33}. \tag{3.17}$$

As noted in Suo (1990), the complex stress intensity factor for this case, however defined, may not reduce to the classical definition as the bimaterial degenerates to the case $\epsilon = 0$, because $\eta \neq 1$ when $v \neq 0$ even for isotropic bimaterials.

A length $\hat{L}$ is used to specify the mode mixity,

$$\tan\hat{\psi} \equiv \left(\frac{\sigma_{12}}{\eta\sigma_{22}}\right)_{r=\hat{L}} = \arg(K\hat{L}^{\mathrm{i}\epsilon}), \quad \cos\phi = \left(\frac{t_3}{|t|}\right)_{r\to 0} = \frac{K_3}{\sqrt{(|K|^2+K_3^2)}}. \tag{3.18}$$

As implied by (3.18), the phase shift due to different lengths, $\hat{L}_1$ and $\hat{L}_2$, is

$$\hat{\psi}_2 - \hat{\psi}_1 = \epsilon \ln(\hat{L}_2/\hat{L}_1). \tag{3.19}$$

The displacement jump is

$$\delta_2 + \mathrm{i}\eta\delta_1 = \frac{H_{22}Kr^{\mathrm{i}\epsilon}}{(1+2\mathrm{i}\epsilon)\cosh\pi\epsilon}\sqrt{\left(\frac{2r}{\pi}\right)}, \quad \delta_3 = H_{33}K_3\sqrt{\left(\frac{2r}{\pi}\right)} \tag{3.20}$$

and the energy release rate is related to $K$ and $K_3$ by

$$\mathscr{G} = (\mathscr{F}/4C_{66}^{(1)})\,|K|^2 + \tfrac{1}{4}H_{33}K_3^2. \tag{3.21}$$

We shall refer to the dimensionless real parameter $\mathscr{F}$, pertaining to the in-plane deformation, as the *energy factor*. It has the explicit form

$$\mathscr{F} = C_{66}^{(1)}(H_{22} - H_{12}^2/H_{11}). \tag{3.22}$$

These parameters as a function of the crack speed will be discussed later.

3.2.3. *Angular functions for isotropic bimaterials*

The potential vector $\boldsymbol{f}(z) = \{f_1(z), f_2(z), f_3(z)\}$ for the crack tip field is (Suo 1990)

$$\boldsymbol{L}\boldsymbol{f}'(z) = \frac{\mathrm{e}^{\pi\epsilon}K z^{\mathrm{i}\epsilon}\boldsymbol{w} + \mathrm{e}^{-\pi\epsilon}\bar{K}z^{-\mathrm{i}\epsilon}\bar{\boldsymbol{w}}}{2\cosh\pi\epsilon\,\sqrt{(2\pi z)}} + \frac{K_3\,\boldsymbol{w}_3}{2\sqrt{(2\pi z)}}. \tag{3.23}$$

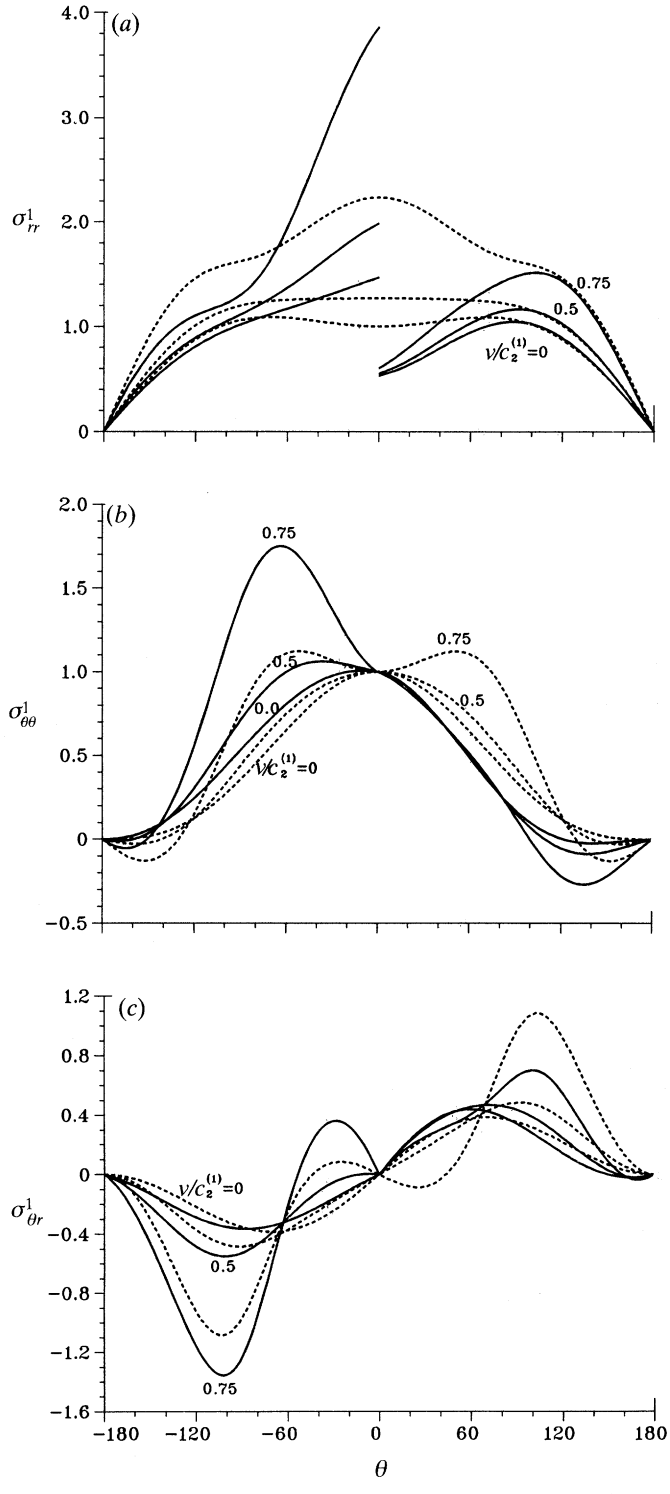


Figure 2. Mode 1 angular functions for the singularity fields of a dynamic interface crack. (*a*) radial stress, (*b*) hoop stress and (*c*) shear stress. (*a*)–(*c*) – – –, $\lambda = 1$; ——, $\lambda = 10$.

This is valid for material 1. The corresponding solution for material 2 is obtained by replacing $\pi\epsilon$ by $-\pi\epsilon$. Each of $f_q(z_q)$ has the form

$$f_q'(z_q) = \frac{1}{2\sqrt{(2\pi z_q)}}\left(\frac{e^{\pi\epsilon}K z_q^{i\epsilon}}{\cosh\pi\epsilon}\boldsymbol{l}_q\cdot\boldsymbol{w} + \frac{e^{-\pi\epsilon}\bar{K} z_q^{-i\epsilon}}{\cosh\pi\epsilon}\boldsymbol{l}_q\cdot\bar{\boldsymbol{w}} + K_3\boldsymbol{l}_q\cdot\boldsymbol{w}_3\right), \tag{3.24}$$

where $\boldsymbol{l}_q$, represents the $q$th row of the matrix $\boldsymbol{L}^{-1}$.

For isotropic materials, the following explicit angular distributions are obtained. For $0 \leqslant \theta \leqslant \pi$,

$$\begin{aligned}
\tilde{\sigma}^1_{11}(\theta) &= (D\cosh\pi\epsilon)^{-1}\{(1+2\alpha_1^2-\alpha_2^2)\gamma_1^{-\frac{1}{2}}(P_{11}\cos\epsilon_1\cos\tfrac{1}{2}\theta_1 + P_{12}\sin\epsilon_1\sin\tfrac{1}{2}\theta_1) + \\
&\quad 2\alpha_2\gamma_2^{-\frac{1}{2}}(P_{21}\cos\epsilon_2\cos\tfrac{1}{2}\theta_2 + P_{22}\sin\epsilon_2\sin\tfrac{1}{2}\theta_2)\}, \\
\tilde{\sigma}^1_{12}(\theta) &= (D\cosh\pi\epsilon)^{-1}\{-2\alpha_1\gamma_1^{-\frac{1}{2}}(P_{12}\sin\epsilon_1\cos\tfrac{1}{2}\theta_1 - P_{11}\cos\epsilon_1\sin\tfrac{1}{2}\theta_1) \\
&\quad + (1+\alpha_2^2)\gamma_2^{-\frac{1}{2}}(P_{21}\cos\epsilon_2\sin\tfrac{1}{2}\theta_2 - P_{22}\sin\epsilon_2\cos\tfrac{1}{2}\theta_2)\}, \\
\tilde{\sigma}^1_{22}(\theta) &= (D\cosh\pi\epsilon)^{-1}\{-(1+\alpha_2^2)\gamma_1^{-\frac{1}{2}}(P_{11}\cos\epsilon_1\cos\tfrac{1}{2}\theta_1 + P_{12}\sin\epsilon_1\sin\tfrac{1}{2}\theta_1) \\
&\quad - 2\alpha_2\gamma_2^{-\frac{1}{2}}(P_{21}\cos\epsilon_2\cos\tfrac{1}{2}\theta_2 + P_{22}\sin\epsilon_2\sin\tfrac{1}{2}\theta_2)\}, \\
\tilde{\sigma}^2_{11}(\theta) &= (D\cosh\pi\epsilon)^{-1}\{(1+2\alpha_1^2-\alpha_2^2)\gamma_1^{-\frac{1}{2}}(P_{12}\cos\epsilon_1\sin\tfrac{1}{2}\theta_1 - P_{11}\sin\epsilon_1\cos\tfrac{1}{2}\theta_1) \\
&\quad + 2\alpha_2\gamma_2^{-\frac{1}{2}}(P_{22}\cos\epsilon_2\sin\tfrac{1}{2}\theta_2 - P_{21}\sin\epsilon_2\cos\tfrac{1}{2}\theta_2)\}, \\
\tilde{\sigma}^2_{12}(\theta) &= (D\cosh\pi\epsilon)^{-1}\{-2\alpha_1\gamma_1^{-\frac{1}{2}}(P_{12}\cos\epsilon_1\cos\tfrac{1}{2}\theta_1 + P_{11}\sin\epsilon_1\sin\tfrac{1}{2}\theta_1) \\
&\quad - (1+\alpha_2^2)\gamma_2^{-\frac{1}{2}}(P_{22}\cos\epsilon_2\cos\tfrac{1}{2}\theta_2 + P_{21}\sin\epsilon_2\sin\tfrac{1}{2}\theta_2)\}, \\
\tilde{\sigma}^2_{22}(\theta) &= (D\cosh\pi\epsilon)^{-1}\{-(1+\alpha_2^2)\gamma_1^{-\frac{1}{2}}(P_{12}\cos\epsilon_1\sin\tfrac{1}{2}\theta_1 - P_{11}\sin\epsilon_1\cos\tfrac{1}{2}\theta_1) \\
&\quad - 2\alpha_2\gamma_2^{-\frac{1}{2}}(P_{22}\cos\epsilon_2\sin\tfrac{1}{2}\theta_2 - P_{21}\sin\epsilon_2\cos\tfrac{1}{2}\theta_2)\}, \\
\tilde{\sigma}^3_{\alpha 3}(\theta) &= \frac{1}{\sqrt{\gamma_3}}\begin{Bmatrix} -\alpha_3^{-1}\sin\tfrac{1}{2}\theta_3 \\ \cos\tfrac{1}{2}\theta_3 \end{Bmatrix},
\end{aligned} \tag{3.25}$$

where the coefficients $P_{\alpha\beta}$ are

$$\left.\begin{aligned}
P_{11} &= (1+\alpha_2^2)\cosh\epsilon(\pi-\theta_1) - 2\eta\alpha_2\sinh\epsilon(\pi-\theta_1), \\
P_{12} &= (1+\alpha_2^2)\sinh\epsilon(\pi-\theta_1) - 2\eta\alpha_2\cosh\epsilon(\pi-\theta_1), \\
P_{21} &= \eta(1+\alpha_2^2)\sinh\epsilon(\pi-\theta_2) - 2\alpha_1\cosh\epsilon(\pi-\theta_2), \\
P_{22} &= \eta(1+\alpha_2^2)\cosh\epsilon(\pi-\theta_2) - 2\alpha_1\sinh\epsilon(\pi-\theta_2).
\end{aligned}\right\} \tag{3.26}$$

For $-\pi \leqslant \theta \leqslant 0$, simply change $\pi$ to $-\pi$ in (3.25) and (3.26). The factors introduced in (3.25) are defined below,

$$\left.\begin{aligned}
\gamma_1 = \sqrt{\left(1-\frac{\rho v^2\sin^2\theta}{C_{11}}\right)}, \quad \gamma_2 = \sqrt{\left(1-\frac{\rho v^2\sin^2\theta}{C_{66}}\right)}, \quad \gamma_3 = \sqrt{\left(1-\frac{\rho v^2\sin^2\theta}{C_{44}}\right)}, \\
\epsilon_j = \epsilon\ln\gamma_j, \quad \tan\theta_j = \alpha_j\tan\theta,
\end{aligned}\right\} \tag{3.27}$$

and the Rayleigh wave function $D$ is given by equation (2.31).

We have recovered the limits for dynamic cracks in homogeneous materials in Freund (1990), and the static interface cracks in Rice *et al.* (1990). The resolution factor $\eta$ causes a minor modification in the angular functions for mode 2 in the former.

The angular functions in (3.25) are plotted in figures 2 and 3. The stiffness ratio $\lambda = C_{66}^{(2)}/C_{66}^{(1)}$ considered is $\lambda = 1$ (homogeneous) and $\lambda = 10$ (strongly mismatched). For simplicity, we take

$$\nu^{(1)} = \nu^{(2)} = 0.3, \quad \rho^{(1)} = \rho^{(2)}. \tag{3.28}$$

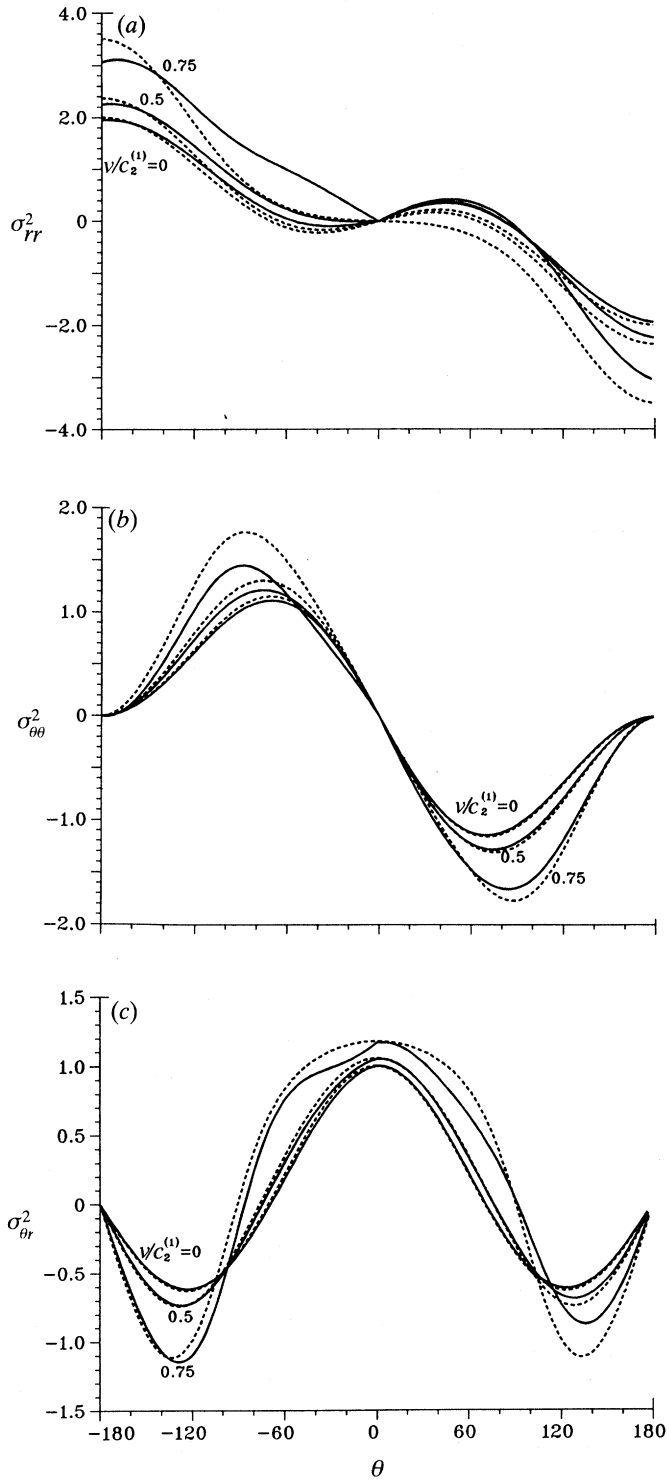


Figure 3. Mode 2 angular functions for the singularity fields of a dynamic interface crack. (*a*) radial stress, (*b*) hoop stress and (*c*) shear stress. (*a*)–(*c*) ----, $\lambda = 1$; ——, $\lambda = 10$.

Curves are shown for various speeds, $v/c_2^{(1)}$, where $c_2^{(1)} = \sqrt{(C_{66}^{(1)}/\rho^{(1)})}$ is the shear wave speed of material 1.

Focus on the hoop stress under mode 1 loading in figure 2*b*. The stress maximum at high speeds, at about 60° from the crack plane (dashed line), has been suggested to account for dynamic branching in homogeneous materials. The even larger maximum in the stiffer substrate (solid curve) would suggest that interface crack may have stronger tendency to branch. However, the extension-branching competition also involves the toughness ratio of the interface to substrates. When the interface is more brittle than the substrates, the crack would be confined on the interface, regardless of the crack speed or more mixity. This may account for the fast debonding noted by Tippur & Rosakis (1990).

Figure 2*a* shows that at high crack speeds, a large radial stress develops in the stiffer material below the interface. This could cause surface cracks on the substrate as the main crack runs by. Further, the different behaviour of the stress difference, $\sigma_{\theta\theta}-\sigma_{rr}$, can lead to different plastic fields and affect the process of plastic loading and elastic unloading in the upper and lower materials. The curves in figure 3 show that the effect of material mismatch on the mode 2 angular functions is less pronounced.

## 4. Dynamic dependence of interface parameters

### 4.1. *Limits at the Rayleigh wave speed of the more compliant material*

In contrast to the small static values of $\epsilon$, the values at high crack speeds can be large. When the crack speed approaches the Rayleigh wave speed $c_R$ of the relatively compliant substrate, assumed to be material 1,

$$\boldsymbol{H} \approx \boldsymbol{B}^{(1)}. \tag{4.1}$$

Under this condition, material 2 can be regarded as energetically detached. A Rayleigh wave propagates along the surface of material 1, and every component of $\boldsymbol{H}$ becomes infinite.

We show that $\epsilon$ becomes unbounded at Rayleigh wave speed for general anisotropic bimaterials. A similar result was obtained by Atkinson (1977) for isotropic bimaterials. First we notice as a necessary consequence of (2.16), the determinant of the adjoint matrix $\boldsymbol{L}_{\mathrm{adj}}^{(1)}$ would vanish as $v \to c_R$

$$\det\{\boldsymbol{L}_{\mathrm{adj}}^{(1)}(c_R)\} = 0. \tag{4.2}$$

On the other hand, the eigenvalue problem (3.8) can be recast as

$$\det\{\beta\,\mathrm{Re}\,[\boldsymbol{A}^{(1)}\boldsymbol{L}_{\mathrm{adj}}^{(1)}] - \mathrm{i}\,\mathrm{Im}\,[\boldsymbol{A}^{(1)}\boldsymbol{L}_{\mathrm{adj}}^{(1)}]\} = 0 \tag{4.3}$$

using (4.1) and the first expression of (2.14). Combining (4.2) and (4.3) provides the desired result,

$$\beta(c_R) = -1 \quad \text{or} \quad \epsilon(c_R) \to \infty. \tag{4.4}$$

Accordingly, $\epsilon$ will increase rapidly as $v \to v_R$. This suggests that the concept of small scale contact zone, which was proposed for small $\epsilon$ in static interfacial crack problems (Rice 1988), may not be applicable at high crack speeds.

Now we direct our attention to the energy factor $\mathscr{F}$ defined in equations (3.21) and (3.22). For homogeneous materials, it is obvious from (3.22) that

$$\mathscr{F}(c_R) \to \infty. \tag{4.5}$$

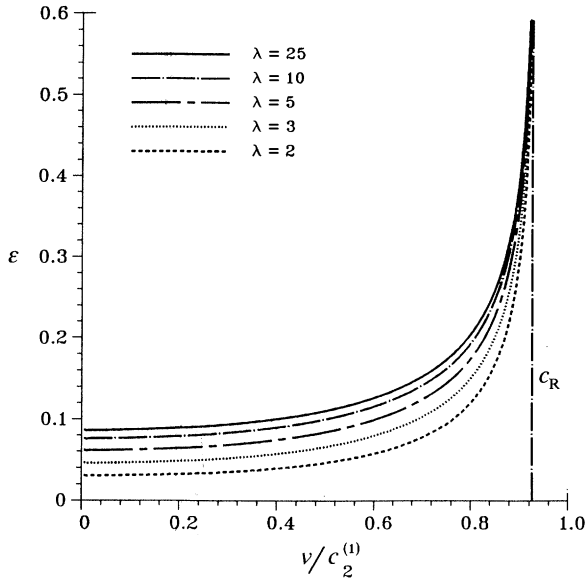


Figure 4. Velocity dependence of oscillation index. The curves are generated for isotropic bimaterials. The two materials have identical density and Poisson's ratio 0.3, $\rho^{(2)} = \rho^{(1)}$. The last solid curve corresponds to the case of $\lambda = 25$ and $\rho^{(2)}/\rho^{(1)} = 3$.

Consequently, in a homogeneous medium, an infinite amount of energy has to be transmitted to the crack tip to maintain its extension at Rayleigh wave speed if the dynamic $K$ is non-zero, or alternatively, a finite energy input to the propagating crack tip requires that $K$ must vanish when the crack speed reaches the Rayleigh wave speed.

A rather different behaviour emerges for interfacial cracks. We found $\mathscr{F}$ is finite at $c_R$, and for aligned orthotropic bimaterials

$$\mathscr{F}(c_R) = \frac{\alpha_1(1-\alpha_2^2)+\alpha_2(1-\alpha_1^2)/b}{\alpha_2(1-\alpha_2^2)\,(\sqrt{(b\alpha_1/\alpha_2)}-\sqrt{(b\alpha_1\alpha_2-1+\alpha_1^2)})}, \quad b = \sqrt{\left(\frac{C_{22}}{C_{11}}\right)}. \tag{4.6}$$

In the above, the elastic constants pertain to the more compliant substrate. For isotropic bimaterials, a simpler result is

$$\mathscr{F}(c_R) = (1-\alpha_1\alpha_2)/\alpha_2(1-\alpha_2^2). \tag{4.7}$$

The boundedness of the energy factor suggests that the dynamic interface stress intensity factors could be non-zero at the lower Rayleigh wave speed.

The traction resolution factor $\eta$ at Rayleigh wave speed is

$$\eta(c_R) = \sqrt{(\alpha_1/b\alpha_2)} = (1+\alpha_2^2)/2\alpha_2. \tag{4.8}$$

The second equality holds if material 1 is isotropic.

### 4.2. *Dependence of interface parameters on crack speed*

Here we consider isotropic bimaterials. The dependence of $\epsilon$, $\eta$ and $\mathscr{F}$ on $\tilde{v}\,(\equiv v/c_2^{(1)})$ is shown in figures 4, 5 and 6, respectively. Note that $\lambda = 1$ corresponds to a homogeneous material. The case of $\lambda = 25$ and $\rho^{(2)}/\rho^{(1)} = 3$, corresponds

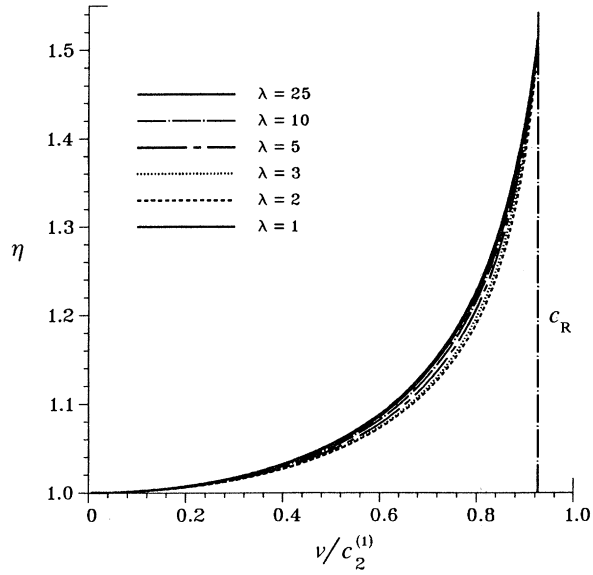


Figure 5. Velocity dependence of traction resolution factor. The curves are generated for isotropic bimaterials with identical density and Poisson's ratio 0.3, and the matching stiffness ratio $\lambda$ is taken as 1, 2, 3, 5 and 10 for the respective curves.

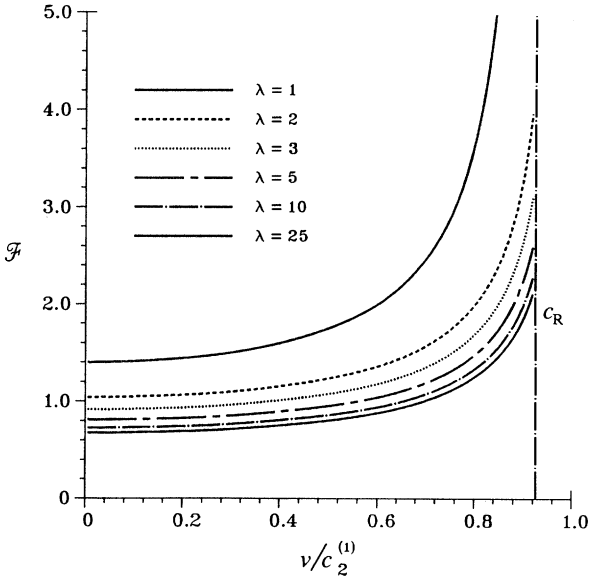


Figure 6. Velocity dependence of energy factor. The curves are generated for isotropic bimaterials with identical density and Poisson's ratio 0.3, and the matching stiffness ratio $\lambda$ is taken as 1, 2, 3, 5 and 10 for the respective curves.

approximately to the PMMA-aluminium interface tested by Tippur & Rosakis (1990). The curves in figure 4 show that $\epsilon$ increases as $\tilde{v}$ increases. When $v \approx 0.8c_R$, as in the above experiment, we note the dynamic $\epsilon$ is about twice the static value. Figure 5 shows that the traction resolution factor $\eta$ depends weakly on $\lambda$ but strongly on $\tilde{v}$.

This implies that the mode mixity shifts as $v$ changes. The distinctly different behaviour of $\mathscr{F}$ for homogeneous materials ($\lambda = 1$) and bimaterials ($\lambda > 1$) is evident from figure 6. The Rayleigh wave speed approximated by

$$c_R/c_2 \approx (0.862 + 1.14\nu)/(1+\nu) \tag{4.9}$$

is marked on figures 4, 5 and 6.

## 5. Stress intensity factors

In this section, dynamic stress intensity factors are catalogued for steady-state problems, including the generalized Yoffe, Gol'dshtein and Dugdale problems. A factorization under time-independent loading is also suggested.

### 5.1. *Steady-state solutions*

#### 5.1.1. *General results*

Figure 7 illustrates a semi-infinite crack and a central crack, both on an interface between two general anisotropic substrates. The steady state is assumed in that the loading and crack configurations are invariant for an observer moving at a constant speed in $x_1$. A constructive approach in Suo (1990) is adopted in the following.

For real $\boldsymbol{H}$, the stress intensity factors are identical to the corresponding crack geometry in homogeneous, isotropic materials under mode III static loading. Thus,

$$\boldsymbol{k} = -\sqrt{\left(\frac{2}{\pi}\right)}\int_{-\infty}^{0} \frac{\boldsymbol{t}(\hat{x}_1)}{\sqrt{-\hat{x}_1}}\,\mathrm{d}\hat{x}_1 \tag{5.1}$$

for the semi-infinite crack, and

$$\boldsymbol{k} = -\sqrt{\left(\frac{1}{\pi a}\right)}\int_{-a}^{a} \sqrt{\left(\frac{a+\hat{x}_1}{a-\hat{x}_1}\right)}\,\boldsymbol{t}(\hat{x}_1)\,\mathrm{d}\hat{x}_1 \tag{5.2}$$

for a Yoffe crack.

For complex $\boldsymbol{H}$, the solution is identical to that for an interface in isotropic bimaterials under static loading:

$$\left.\begin{aligned} K &= -\sqrt{\left(\frac{2}{\pi}\right)}\cosh \pi\epsilon \int_{-\infty}^{0} (-\hat{x}_1)^{-\frac{1}{2}-\mathrm{i}\epsilon}\, t(\hat{x}_1)\,\mathrm{d}\hat{x}_1, \\ K_3 &= -\sqrt{\left(\frac{2}{\pi}\right)}\int_{-\infty}^{0} (-\hat{x}_1)^{-\frac{1}{2}}\, t_3(\hat{x}_1)\,\mathrm{d}\hat{x}_1, \end{aligned}\right\} \tag{5.3}$$

for a semi-infinite crack, and

$$\left.\begin{aligned} K &= -\sqrt{\left(\frac{2}{\pi}\right)}\cosh \pi\epsilon (2a)^{-\frac{1}{2}-\mathrm{i}\epsilon} \int_{-a}^{a} \left(\frac{a+\hat{x}_1}{a-\hat{x}_1}\right)^{\frac{1}{2}+\mathrm{i}\epsilon} t(\hat{x}_1)\,\mathrm{d}\hat{x}_1, \\ K_3 &= -\sqrt{\left(\frac{1}{\pi a}\right)}\int_{-a}^{a} \left(\frac{a+\hat{x}_1}{a-\hat{x}_1}\right)^{\frac{1}{2}} t_3(\hat{x}_1)\,\mathrm{d}\hat{x}_1, \end{aligned}\right\} \tag{5.4}$$

for a Yoffe crack. We emphasize that $t$ and $t_3$ are the generalized tractions as defined as in (3.12), and $t = \sigma_{22} + \mathrm{i}\sigma_{21}/\eta$ for orthotropic bimaterials. Examples below assume the bimaterials are orthotropic.

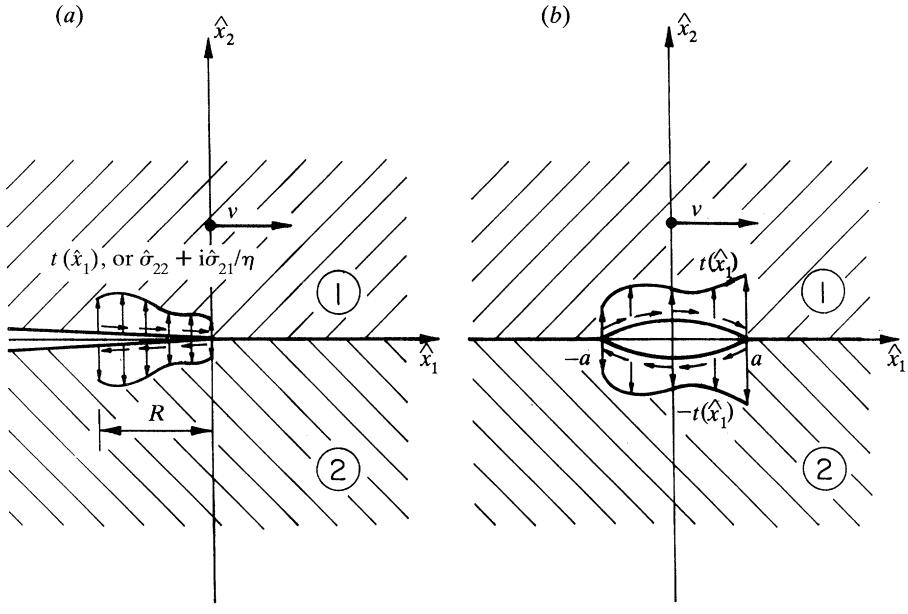


Figure 7. Geometries of steady state growing cracks. (*a*) A semi-infinite crack with a possible translating cohesive zone; (*b*) a central crack.

5.1.2. *Yoffe problem*

Consider the steady state translation of a central crack of fixed length $2a$ subject to remote uniform stresses. The constant negating traction on the crack faces is

$$t = -\sigma_{22}^{\infty} - \mathrm{i}\sigma_{21}^{\infty}/\eta. \tag{5.5}$$

Equation (5.4), reduces to

$$K = (1+2\mathrm{i}\epsilon)\,(2a)^{-\mathrm{i}\epsilon}\,(\sigma_{22}^{\infty} + \mathrm{i}\sigma_{21}^{\infty}/\eta)\,\sqrt{(\pi a)}. \tag{5.6}$$

The mode mixity is

$$\hat{\psi} = \arctan\,(\sigma_{21}^{\infty}/\eta\sigma_{22}^{\infty}) + \epsilon \ln\,(\hat{L}/2a) + \arctan\,(2\epsilon). \tag{5.7}$$

The effect of elastic mismatch, anisotropy and crack speed on the magnitude and phase angle of the complex stress intensity factor can be seen.

5.1.3. *Gol'dshtein problem*

The interface crack is loaded by opposing point forces $P$ and $Q$ which translate as the crack advances. Equation (5.3) reduces to

$$K = \sqrt{(2/\pi L)}\,(P + \mathrm{i}Q/\eta)\,L^{-\mathrm{i}\epsilon}\cosh \pi\epsilon. \tag{5.8}$$

The phase angle is

$$\hat{\psi} = \arctan\,(Q/\eta P) + \epsilon \ln\,(\hat{L}/L). \tag{5.9}$$

5.1.4. *Dugdale problem*

Fracture resistance can originate from a variety of sources: craze in polymers, ductile reinforcement in ceramics, bridging fibres in composites, etc. For these mechanisms to operate, energy dissipates in the damage localized on the planar zone ahead of the crack tip. We consider crack tip shielding by a translating damage zone as depicted in figure 7*a*.

For simplicity, the bridging zone length, $R$, is assumed to be small compared with

the overall specimen size. The crack and the damage zone are advancing under steady-state conditions. Thus the overall geometry and the applied load can be characterized by a far field stress intensity factor, $K_{\text{appl}}$. The stress intensity factor at the crack tip is shielded by the damage zone, in accordance with

$$K_{\text{appl}} - K_{\text{tip}} = \sqrt{\left(\frac{2}{\pi}\right)} \cosh \pi\epsilon \int_{\hat{x}_1=-R}^{\hat{x}_1=0} (-s)^{-\frac{1}{2}-\mathrm{i}\epsilon} [\hat{\sigma}_{22}(s) + \mathrm{i}\hat{\sigma}_{21}(s)/\eta] \, \mathrm{d}s, \tag{5.10}$$

where $\hat{\sigma}_{2\alpha}$ are the closure tractions, and $K_{\text{tip}}$ the stress intensity factor at the crack tip.

Assume both $\hat{\sigma}_{22}$ and $\hat{\sigma}_{21}$ are constant over the damage zone. The general formula (5.10) reduces to

$$K_{\text{appl}} - K_{\text{tip}} = 2\sqrt{\left(\frac{2R}{\pi}\right)} \frac{\cosh \pi\epsilon}{1-2\mathrm{i}\epsilon} R^{-\mathrm{i}\epsilon} [\hat{\sigma}_{22} + \mathrm{i}\hat{\sigma}_{21}/\eta]. \tag{5.11}$$

Depending on the material response, the crack tip may dissipate energy ($K_{\text{tip}} \neq 0$), or may not ($K_{\text{tip}} = 0$). For the latter case, we equate the amplitude and phase angle of the two sides in (5.11) to get

$$R = \frac{8}{\pi} \frac{(1+4\epsilon^2)\,|K_{\text{appl}}|^2}{\cosh^2(\pi\epsilon)\,(\hat{\sigma}_{22}^2 + \hat{\sigma}_{21}^2/\eta^2)} \tag{5.12}$$

and

$$\arctan(\hat{\sigma}_{21}/\hat{\sigma}_{22}\,\eta) = \hat{\psi}_{\text{appl}} + \epsilon \ln(R/\hat{L}) - \arctan 2\epsilon, \tag{5.13}$$

where $\hat{\psi}_{\text{appl}} = \arg(K_{\text{appl}}\,\hat{L}^{\mathrm{i}\epsilon})$.

Now suppose the two closure stresses are connected by a condition similar to a yield criterion, i.e.

$$F(\hat{\sigma}_{22}/\sigma_{\text{s}}, \hat{\sigma}_{21}/\sigma_{\text{s}}) = 0 \tag{5.14}$$

where $F$ is a dimensionless function, and $\sigma_{\text{s}}$ is the yield stress. Equations (5.13) and (5.14) can be used to determine the magnitude of the closure stresses. The present solution degenerates to that of Ortiz & Blume (1990) for a static crack in an isotropic bimaterial.

### 5.2. *K-factorization under time-independent loading*

Another important category is dynamic crack growth under a time-independent loading. For a general non-uniform crack motion in a homogeneous, isotropic unbounded medium (or before the reflection waves reach the crack tip), the dynamic stress intensity factor at the instantaneous crack length $l$ and crack speed $v$ can be factored into (see Freund 1990)

$$K_{\text{I}}(l, v) = k_{\text{I}}(v)\, K_{\text{I}}(l, 0), \tag{5.15}$$

where $K_{\text{I}}(l, 0)$ is the static stress intensity factor at the instantaneous crack length $l$, and $k_{\text{I}}(v)$ is a universal function of $v$. Similar factorizations hold for the other two modes. In the following we seek to extend the above result to interface cracks in anisotropic bimaterials.

Consider a stationary crack subjected to time-independent load. At $t = 0$, the crack starts to run at a constant speed $v$. We seek the connection between the stress intensity factor for the stationary crack, $K(l, 0)$ and the dynamic stress intensity factor $K(l, v)$. Attention is restricted to small-scale disturbance, i.e., crack extension $vt$ is small compared with the overall specimen size. Observe $vt$ is the only length in the problem. Dimensionality and linearity require

$$K(l, v) = (vt)^{-\mathrm{i}\epsilon} [(vt)^{\mathrm{i}\epsilon_0} K(l, 0)\, k_1(v) + (vt)^{-\mathrm{i}\epsilon_0} \bar{K}(l, 0)\, k_2(v)]. \tag{5.16}$$

Here $\epsilon_0$ is the static oscillation index, $\epsilon$ the oscillation index at crack speed $v$, and $k_1$ and $k_2$ dimensionless functions that depend on $v$ and the elastic constants, but independent of specimen geometry. The two functions are complex-valued and can in principle be extracted from the solution to a boundary-value problem.

## 6. Concluding remarks

This study is a first step towards building a body of results that could serve to broaden the interface fracture mechanics to include aspects of high loading rates, rapid crack propagation and strain rate dependent material response. The presentation of the dynamics of high-speed debonding emphasizes concepts which unify both static interface fracture and dynamic fracture in homogeneous materials. The steady state nature of the near-tip singularity suggests debonding resistance should be viewed as speed dependent, if higher-order terms are ignored. Careful experiments are called for to determine the fracture resistance to high speed debonding, to address issues such as material strain rate sensitivity, inertia effects, etc.

The generation of fracture resistance data for the full range of mode mixities requires opening dominated, sliding dominated and mixed mode test specimens. Explicit results provided in this paper may serve as basis for specimen calibration. Priority should be given to developing test specimens that can generate experimental data, and are convenient for the analysis of the fracture process, e.g. crack tip motion against time and applied displacement or load histories. Exchanges between experimentalists and analysts are vital to designing effective test specimens.

For composite laminates, *in situ* observation of the high-speed damage progression will help to model, and eventually to design against failure. Explicit results provided in this paper can guide micromechanical modelling. Further mechanics studies along these lines including the analysis of transient debonding problems are in progress.

W. Y. and C. F. S. are supported by the Office of Naval Research through ONR Grant N00014-90-J1380. Z. S. is supported by a NSF research initiative award (MSS-9011571), and by an ONR/URI contract (N00014-86-K-0753). The computations were carried out at the Computational Mechanics Research Facility within the Division of Engineering of Brown University. The visit of W. Y. to Brown University was made possible also by the support from the Fok Ying Tung Education Foundation.

## References

Atkinson, C. 1977 Dynamic crack problems in dissimilar media. In *Mechanics of fracture 4: elastodynamic crack problems* (ed. G. C. Sih), pp. 213–248. Leyden: Noordhoff.

Barnett, D. M., Lothe, J., Gavazza, S. D. & Musgrave, M. J. P. 1985 Considerations of the existence of interfacial (Stoneley) waves in bounded anisotropic elastic half-spaces. *Proc. R. Soc. Lond.* A **402**, 153–166.

Evans, A. G., Rugle, M., Dalgleish, B. J. & Charalambides, P. G. 1990 The fracture energy of bimaterial interfaces. *Mater. Sci. Engng* A **126**, 53–64.

Freund, L. B. 1990 *Dynamic fracture mechanics*. Cambridge University Press.

Gol'dshtein, R. V. 1966 On the steady motion of a crack along a straight line boundary between two joined materials. *Inzh. Zh. MTT* **5**, 93–101.

Hutchinson, J. W. & Suo, Z. 1991 Mixed mode cracking in layered materials. In *Advances in applied mechanics* **28** (ed. J. W. Hutchinson & T. Y. Wu). New York: Academic Press. (In the press.)

Ingebrigtsen, K. A. & Tonning, A. 1969 *Phys. Rev.* **184**, 942–951.

Irwin, G. R. 1960 Fracture Mechanics. In *Structural Mechanics* (ed. J. N. Goodier & N. J. Hoff), pp. 557–591. New York: Pergamon.

Lothe, J. & Barnett, D. M. 1976 On the existence of surface wave solutions for anisotropic elastic half-spaces with free surface. *J. appl. Phys.* **47**, 428–433.

Ortiz, M. & Blume, J. A. 1990 Effect of decohension and sliding on bimaterial crack-tip fields. *Int. J. Fracture* **42**, 117–128.

Rice, J. R. 1968 Mathematical analysis in the mechanics of fracture. In *Fracture*, vol. 2 (ed. H. Liebowitz), pp. 191–311. New York: Academic Press.

Rice, J. R. 1988 Elastic fracture mechanics concepts for interfacial cracks. *J. appl. Mech.* **55**, 98–103.

Rice, J. R., Suo, Z. & Wang, J. S. 1990 Mechanics and thermodynamics of brittle interfacial failure in bimaterial systems. In *Metal–ceramic interfaces. Acta-Scripta Metallurgica Proc. Ser.* **4**, pp. 269–294. New York: Pergamon Press.

Ruhle, M., Evans, A. G., Ashby, M. F. & Hirth, J. P. 1990 *Metal–ceramic interfaces. Acta-Scripta Metallurgica Proc. Ser.* **4**. New York: Pergamon Press.

Stroh, A. N. 1962 Steady state problems in anisotropic elasticity. *J. Math. Phys.* **41**, 77–103.

Suo, Z. 1990 Singularities, interfaces and cracks in dissimilar anisotropic media. *Proc. R. Soc. Lond.* A **427**, 331–358.

Ting, T. C. T. 1986 Explicit solution and invariance of the singularities at an interface crack in anisotropic composites. *Int. J. Solids Struct.* **22**, 965–983.

Tippur, V. H. & Rosakis, A. J. 1990 Quasi-static and dynamic crack growth along bimaterial interface: a note on crack tip measurements using coherent gradient sensing. In *SM Rep. 90-17*. California Institute of Technology.

Wang, T. C., Shih, C. F. & Suo, Z. 1991 Mechanics of interface crack extension and kinking in anisotropic solids. *Int. J. Solids Struct.* (In the press.)

Willis, J. R. 1971 Fracture mechanics of interfacial cracks. *J. Mech. Phys. Solids* **19**, 353–368.

Wu, K. C. 1991 Explicit crack-tip fields of an extending interface crack in an anisotropic bimaterial. *Int. J. Solids Struct.* **27**, 455–466.

Yoffe, E. H. 1951 The moving Griffith crack. *Phil. Mag.* **42**, 739–750.

*Received 23 November 1990; accepted 10 January 1991*